Planet. Space Sci., Vol. 30, No. 11, pp. 1091–1105, 1982
Printed in Great Britain

0032-0633/82/111091-15$03.00/0
Pergamon Press Ltd.

TRANSPORT OF AURORALLY PRODUCED N(^{2}D) BY WINDS IN THE HIGH LATITUDE THERMOSPHERE

J.-C. GÉRARD
Institut d'Astrophysique, Université de Liège, 4200 Liège, Belgium

and

R. G. ROBLE
National Center for Atmospheric Research,* P. O. Box 3000, Boulder, CO 80307, U.S.A.

(Received 27 April 1982)

Abstract—A time-dependent two-dimensional numerical model of the minor neutral constituents of the thermosphere NO, N(^{2}D), and N(^{4}S) is used to examine the effects of winds in transporting these constituents from their production region in auroral arcs. The calculations show that thermospheric winds flowing through regions of enhanced local auroral production produce downwind plumes of enhanced minor neutral constituent densities and that the densities depend upon the wind velocity. Below about 200 km N(^{2}D) is in photochemical equilibrium and is not transported. Above 200 km N(^{2}D) is transported by the wind and since quenching of N(^{2}D) by O is small and the radiational lifetime is long, a downwind plume of emission at 5200 Å develops from the particle source region. We present data from a rocket flight in the vicinity of the magnetospheric cusp and data from the Atmosphere Explorer-D (AE-D) satellite that both show enhanced 5200 Å emission rates in a general downwind direction from a region of direct particle precipitation. The general wind speed and direction are obtained from predictions made by the NCAR thermospheric general circulation model. The results suggest that transport of N(^{2}D) by the wind system is more important than the convection of O^+ ions by electric fields in causing the enhanced 5200 Å emission rate in regions outside but in the vicinity of direct particle precipitation.

1. INTRODUCTION

Meridional circulation driven by differential solar and high latitude heating is known to redistribute thermospheric inert and long-lived constituents. On a local scale, horizontal transport by neutral winds may also affect the distribution of minor constituents, especially in the presence of localized or structured sources. This is the case in the auroral zones, where there are large horizontal gradients in the ionization and production field together with substantial thermospheric winds.

The importance of transport by horizontal wind of aurorally produced metastable $O_2(^1\Delta_g)$ molecules has been studied by Rees and Roble (1980). The O_2 $^1\Delta$ state has a radiative lifetime of about 1 hr and is not subject to collisional quenching. Therefore metastable O_2 may be transported away from an auroral arc by a horizontal wind and the downwind 1.27 μm emission from this state would be considerably higher than under the no-wind conditions. Large O_2 1.27 μm/N_2^+ 4278 Å airglow emission ratios have been observed, which is most likely due to horizontal transport of the long lived excited species from the auroral source region.

The three major thermospheric odd nitrogen species NO, N(^{4}S) and N(^{2}D), which have long chemical lifetimes, are enhanced by particle precipitation and are therefore subject to horizontal transport. Roble and Gary (1979) studied the local effects of horizontal transport by a neutral wind on the auroral NO-N(^{4}S) system in the lower thermosphere with a time-dependent two-dimensional model. They showed that both species are carried downwind over considerable distances in the vicinity of an auroral arc. In their model, the NO density inside the arc is decreased by a factor of 2.6 as nitric oxide molecules are removed by the wind. However, transport was considered only for NO and N(^{4}S) and N(^{2}D) was assumed to be in photochemical equilibrium in the lower thermosphere. Shepherd *et al.* (1976) presented observational evidence for horizontal transport of N(^{2}D) at higher altitudes near the dayside polar cusp. They reported that rocket measurements of the [NI] ^{4}S–^{2}D 5200 Å emission showed a long tail of N(^{2}D) stretching poleward of the cusp precipitation region. They attributed this delocaliza-

*The National Center for Atmospheric Research is sponsored by the National Science Foundation.

tion to the effect of a day- to night-side neutral wind or to antisolar convection of ions by the electric field. These measurements are described in detail and modeled in a later section of this paper. Further observations of the polar 5200 Å morphology have been described by Frederick and Hays (1978). They mapped the geographic distribution of the column overhead intensity of the NI 5200 Å and N_2 first positive (1P) emissions measured with the Visible Airglow Experiment on the Atmosphere Explorer-C (AE-C) satellite. The measurements were made in early 1975 when the spacecraft was in a nearly circular orbit at 240 km and were confined to regions at invariant latitudes, Λ, of 65–80°. The N_2 1P bands are mostly excited by low energy (10–40 eV) electrons which are in either the soft primary or secondary spectrum. The $N(^2D)$ 5200 Å emission is caused by a number of direct as well as indirect excitation processes (Rusch *et al.*, 1975; Frederick and Rusch, 1977; Rusch and Gérard, 1980; Gérard, 1980). The N_2 1P emission showed a spiked structure, whereas the 5200 Å emission exhibited a much smoother distribution. Frederick and Hays attributed this smearing to a flow of O^+ ions induced by the convection electric field followed by the $O^+ + N_2 \rightarrow NO^+ + N(^4S)$ and $NO^+ + e \rightarrow N(^2D) \rightarrow O$ reactions occurring out of the primary precipitation region.

In this study, we present results of a two-dimensional model calculation illustrating the effect of vertical and horizontal transport on the distribution of aurorally produced $N(^2D)$, $N(^4S)$ and NO. We present results of the rocket measurement of the 5200 Å distribution near the day-side polar cusp and compare them with model calculations. Further observations of the 5200 Å auroral intensity by the Atmosphere Explorer-D (AE-D) satellite show transport effects in the vicinity of both the day- and night-side auroral ovals. Our calculations indicate that thermospheric winds with velocities of 100–300 ms^{-1} are needed to explain both the rocket and satellite observations. Such wind velocities are consistent with theoretical calculations made by a three-dimensional model of thermospheric circulation at solstice during quiet magnetic conditions.

2. MODEL

The basic two-dimensional numerical model used to determine the effect of transport on the minor neutral constituents in the thermosphere has been described previously by Roble and Gary (1979). They considered the transport of only NO and $N(^4S)$ in the lower thermosphere and assumed that $N(^2D)$ was in photochemical equilibrium. We have extended the model upward in altitude to consider the transport of the three minor neutral constituents NO, $N(^4S)$, and $N(^2D)$ for this study. Other changes included in the model described by Roble and Gary (1979) are as follows: (a) the height range is $90 \leq Z \leq 390$ km; (b) the horizontal grid is changed to spherical coordinates covering a latitude range from 75 to 85°N; (c) zero vertical flux values are assumed for NO, $N(^4S)$, and $N(^2D)$ along both the upper and lower horizontal boundaries; (d) a natural flow of constituents out of the downstream lateral boundary is assumed; and (e) the background atmosphere is specified by the Mass Spectrometer and Incoherent Scatter (MSIS) empirical model of atmospheric temperature and composition (Hedin *et al.*, 1977a, 1977b) above 120 km and blended into a standard atmosphere below 120 km. The model has also been extended to include a self-consistent coupled ionosphere. The model ionosphere assumes that N_2^+, O_2^+, and NO^+ are in photochemical equilibrium but that O^+ can diffuse vertically. The chemical reactions and rates for the model ionosphere are the same as used by Torr *et al.* (1979). Horizontal transport of the ion species is not considered in the model. The neutral and ion chemistry in the model and the reaction rate coefficients are listed in Table 1.

The model calculations simulate high latitude phenomena in the winter hemisphere and therefore a small background ionization rate due to scattered Lyman-β (Ly-β) and other nightglow emissions is assumed to establish the background initial distribution of the minor neutral and ion constituents in the thermosphere. A steady neutral wind is assumed to be flowing across the grid from low to high latitudes. The wind profile is obtained from the NCAR thermospheric general circulation model and is typical of high latitude conditions during quiet and moderate levels of geomagnetic activity (Dickinson *et al.*, 1981; Roble *et al.*, 1981). At time $t = 0$ we superimpose an aurora over a portion of the grid and calculate the downwind transport of the minor neutral constituents for a 3 h time period. During this time we assume that the aurora is steady and the ion and minor neutral constituent production rates are constant. It is also assumed that the aurora is spatially small and the local atmospheric response generated by particle heating in the aurora does not interact with the basic flow driven by global pressure gradients. The horizontal flow is assumed to be uniform during the simulation; however, the vertical wind due to adiabatic expansion of the atmosphere as des-

TABLE 1. CHEMICAL REACTIONS AND RATE COEFFICIENTS USED IN THE MODEL

No.	Reaction	Rate coefficient (cm^3s^{-1})	Reference
1	$N(^4S)+O_2\rightarrow NO+O$	$2.4\times10^{-11}\exp(3975/T_n)$	Wilson (1967)
2	$N(^2D)+O_2\rightarrow NO+O$	6×10^{-12}	Frederick and Rusch (1977)
3	$N(^4S)+NO\rightarrow N_2+O$	$1.5\times10^{-12}\,T^{1/2}$	Philip and Schiff (1962)
4	$N(^2D)+NO\rightarrow N_2+O$	7×10^{-11}	Black *et al.* (1969)
5	$N(^2D)+O\rightarrow N(^4S)+O$	4.0×10^{-13}	Frederick and Rusch (1977)
6	$N(^2D)\rightarrow N(^4S)+h\nu$	$1.07\times10^{-5}(s^{-1})$	
7	$N(^2D)+e\rightarrow N(^4S)+e$	$3.6\times10^{-10}(T_e/300)^{1/2}$	Frederick and Rusch (1977)
8	$O_2^++NO\rightarrow NO^++O_2$	4.4×10^{-10}	Lindinger *et al.* (1975)
9	$N_2^++e\rightarrow N(^2D)+N(^4S)$	$1.8\times10^{-7}\,(T_e/300)^{-0.39}$	Mehr and Biondi (1969)
10	$O^++N_2\rightarrow NO^++N(^4S)$	$1.533\times10^{-12}-5.92\times10^{-13}$ $(T_{eff}/300)+8.6\times10^{-14}(T_{eff}/300)^2$	Torr and Torr (1979)
11	$NO^++e\rightarrow O+N(^2D,\,^4S)$	$4.2\times10^{-7}\,(T_e/300)^{-0.85}$	Torr and Torr (1979)
12	$O_2^++N(^4S)\rightarrow NO^++O$	1.8×10^{-10}	Goldan *et al.* (1966)
13	$N_2^++O\rightarrow NO^++N(^2D)$	$1.4\times10^{-10}\,(T_n/300)^{-0.44}$	Torr and Torr (1979).

The electron impact branching ratio is assumed to be 50% N(²D) and 50% N(⁴S).

cribed by Hays *et al.* (1973b) is calculated and included in the model simulation.

3. MODEL AURORAL RESULTS

To illustrate the effect of transport on the distribution of minor neutral constituents in the auroral regions we present some model calculations with simplified auroral structures. A uniform horizontal meridional wind with a vertical profile approximated by

$$v(Z)=v_\infty-(v_\infty-v_0)\exp[-(Z-Z_0)/\mathrm{H}], \quad (1)$$

where v_0 is set to zero at $Z_0=90$ km, H is 100 km and v_∞ is an exospheric wind velocity that varies for different model runs and the wind is assumed to be flowing from low to high latitudes. This velocity profile is an approximation to the meridional wind flow determined at high latitudes during daytime conditions from the NCAR thermospheric general circulation model (Dickinson *et al.*, 1981; Roble *et al.*, 1981). This wind is driven by large horizontal scale pressure gradients generated by solar and high latitude heating as part of the circulation of the thermosphere. In these calculations it is assumed that the heating due to the aurora directly goes into adiabatic expansion (Hays *et al.*, 1973b) and the vertical winds generated by the heating are superimposed upon the basic flow.

The model aurora assumes a horizontal Gaussian flux distribution according to

$$F(\theta)=F_0\exp(-(\theta-\theta_0)^2/\mathrm{H}_\theta^2), \quad (2)$$

where θ_0 is 75.5°N and H_θ is 0.5°. The differential number flux is represented by the analytic expression (Belon *et al.*, 1966)

$$N(E)\,dE=N_0E\exp(-E/\alpha)\,dE \quad (3)$$

where the energy E is expressed in keV, the mean energy of the distribution is 2α(keV) and N_0 is the normalization factor such that the total electron flux, F, is

$$F=N_0\alpha^2\ \mathrm{el\,cm^{-2}/s}. \quad (4)$$

The total energy flux is

$$Q=2\alpha F\ \mathrm{keV\,cm^{-2}/s}. \quad (5)$$

We consider two model auroral cases: (a) a soft-flux aurora where $\alpha=0.2$ keV and $F=3.12\times10^9\,\mathrm{cm^{-2}/s}$, giving $Q=2\,\mathrm{erg\,cm^{-2}/s}$ and (b) a harder flux aurora where $\alpha=2.0$ keV and $F=6.24\times10^8\,\mathrm{cm^{-2}/s}$, giving $Q=4\,\mathrm{erg\,cm^{-2}/s}$. The energy degradation of the auroral flux with altitude and the ionization rate of various species are calculated using the procedure given by Rees (1969) and Roble and Rees (1977). The ion densities and minor neutral constituent production rates are calculated using the chemistry given in Table 1. The aurora is assumed to turn on abruptly at time $t=0$ and remain steady. The model is run for 3 h of simulation time.

The results of our calculation for the soft aurora case with and without a meridional thermospheric wind are shown in Fig. 1. The calculated dis-

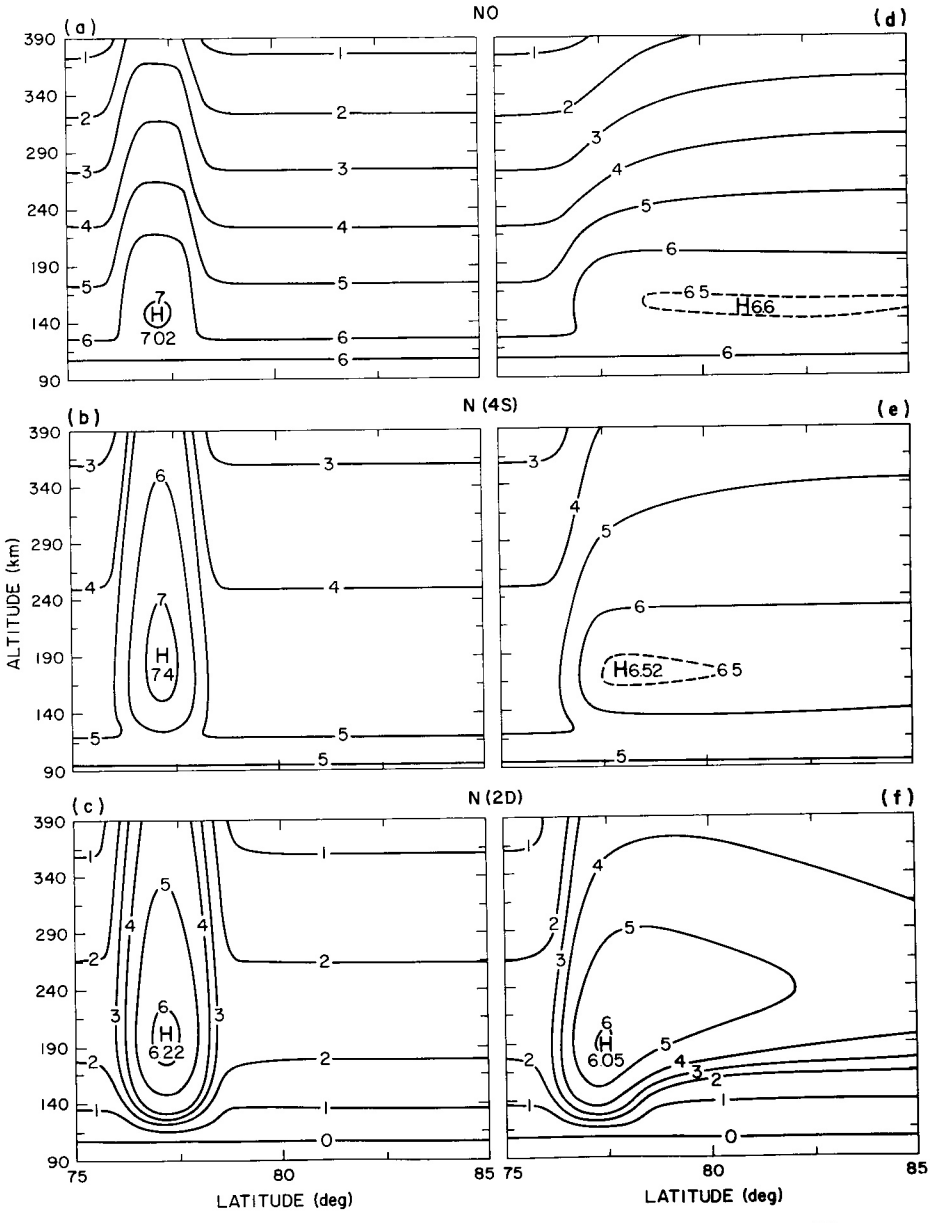

FIG. 1. CONTOURS OF CALCULATED LOG_{10} OF ODD NITROGEN DENSITIES AFTER 3 h OF AURORAL PRECIPITATION CHARACTERIZED BY $\alpha = 2.0$ keV: (a), (b) AND (c) WITHOUT WIND; (d), (e) AND (f) WITH ASYMPTOTIC WIND VELOCITY OF 200 ms^{-1}.

tributions of NO, N(^{4}S), and N(^{2}D) for the no-wind case are shown in Figs. 1a, 1b and 1c, respectively. The densities of all the minor species are enhanced by the aurora and the horizontal distribution variation is similar to the assumed horizontal Gaussian electron flux distribution given by equation (2). The peak NO density occurs in the center of the auroral beam near 140 km with a density of 1.05×10^7 cm^{-3}. The N(^{4}S) density peaks near 180 km with a density of 2.3×10^7 cm^{-3} and the N(^{2}D) density peaks near 210 km with a density of 1.66×10^6 cm^{-3}; both have maximum values in the center of the auroral beam.

The calculated distributions of NO, N(^{4}S) and N(^{2}D) when a meridional wind of the form specified by equation (1) with an exospheric wind

velocity v_∞, of 200 ms^{-1} is included are shown in Figs. 1d, 1e and 1f, respectively. The contours give the minor neutral constituent distributions 3 h after the onset of the aurora particle precipitation. The wind transports each of the minor constituents downwind from the auroral beam producing a compositional enhancement plume. The NO plume in the upper thermosphere extends far downwind from the auroral source region. The chemical reactions for the decay of NO are proceeding slowly, so that there is little decay of NO with distance from the aurora. The N(⁴S) distribution is similar to the NO distribution and it is considerably greater than the calculated background densities in the no-wind case. The NO and N(⁴S) number densities near 180 km are similar in magnitude. The N(²D) downwind plume shown in Fig. 1f shows a decrease in number density from the maximum values that occur in the center of the aurora particle precipitation region. This decrease is due to slow quenching of N(²D) by atomic oxygen to N(⁴S). In Fig. 1e the N(⁴S) contours in the upper thermosphere slope upward, indicating a slight increase in the N(⁴S) density due to the quenching of N(²D) by atomic oxygen. Below about 180 km there is little transport of N(²D) by the winds resulting in a photochemical equilibrium distribution. The downwind transport of the minor constituents also decreases the magnitude of the peak densities from the values calculated in the no-wind case. The peak values of NO decrease from 1.05×10^7 to 3.9×10^6 cm^{-3} and the peak values of N(²D) decrease from 2.3×10^6 to 1.1×10^6 cm^{-3}. The peak value of N(⁴S) shows a much greater decrease due to downwind transport from 2.3×10^7 to 3.3×10^6 cm^{-3}.

The calculated distributions of the minor neutral constituents for the harder aurora case are shown in Fig. 2. In the no-wind case, the enhanced distributions of NO, N(⁴S) and N(²D) are limited to the region of direct particle precipitation as shown in Figs. 2a, 2b and 2c, respectively. The particles from the harder aurora penetrate deeper into the atmosphere and the peak densities of all constituents occur at a lower altitude than in the previous case for the soft aurora. The peak NO density occurs in the center of the auroral beam at 115 km at 1.25×10^8 cm^{-3}. The higher NO densities occur because of the larger N(²D) production rate at low altitudes, as seen by comparing Fig. 2c with 1c, and the rapid reaction of N(²D) with O_2 to produce NO at low altitudes. The peak value of N(²D) is 2.1×10^5 cm^{-3} and it occurs at 180 km in the center of the aurora beam. The N(⁴S) is also produced at a much lower altitude than in the previous case and since NO is the dominant species in the lower thermosphere it destroys N(⁴S). The peak value of N(⁴S) is 10^7 cm^{-3}, and it occurs at 125 km in the center of the aurora.

The effect of winds on the distributions of the minor neutral constituents is shown in Fig. 2d, 2e and 2f. The same wind profile, with v_∞ of 200 ms^{-1}, that was used in the previous case is also used here. The wind velocities are much smaller in the lower thermosphere, and the effect of transport on the minor neutral constituent distributions is less pronounced than in the previous case. The NO is transported downwind in the lower thermosphere, but because of the lower wind velocity in the vicinity of 130 km there is still a downwind gradient of NO density 3 h after the initiation of the aurora. A similar situation develops for N(⁴S); however, in addition to transport there is strong chemical destruction of N(⁴S) by NO downwind of the main particle precipitation region. The chemical destruction occurs because NO is the dominant species at low altitudes and the dominant species, either NO or N(⁴S), chemically destroys the other. Thus a compositional "hole" in the N(⁴S) develops in the lower thermosphere downwind of the aurora due to rapid chemical reactions in a region of no particle production.

The N(²D) distribution is in photochemical equilibrium in the lower thermosphere and the number density distributions are similar for the cases without and with winds as seen in Figs. 1c and 1f and 2c and 2f respectively. Above about 200 km the chemical lifetime of N(²D) becomes longer and there is considerable downwind transport of N(²D). However, there is still sufficient quenching of N(²D) to N(⁴S) mainly by atomic oxygen so that the N(²D) density decreases and N(⁴S) density increases slightly with horizontal distance from the aurora.

4. N(²D) TRANSPORT IN THE CUSP REGION

Observations

The N(²D) 5200 Å emission was measured in the polar cap by the University of Liège photometer aboard a Black Brant V rocket launched from Cape Parry (North West Territories) at 23:32:06 U.T. on 6 December 1974. The launch azimuth was 44°E, which is approximately parallel to the magnetic meridian. The geographic coordinates of the launch site are 70.2°N and 124.7°W. The relatively low elevation angle of 74.2° was such that the horizontal range of the rocket reached about 500 km. The rocket remained above 100 km in

TABLE 2. PARAMETERS FOR ROCKET AND ATMOSPHERE EXPLORER D OBSERVATIONS*

Orbit	Day	U.T.	Latitude (°N)	Solar zenith angle	Local solar time	A_p
419D†	315–1975	1843	73.8	123°	22.9 h	13
491D	321–1975	2221	87.2	112°	22.6 h	17
494S	322–1975	0425	87.1	112°	22.6 h	7
Rocket	341–1974	2336	72	102°	14.8 h	4

*Parameters refer to perigee for the AE-D satellite and apogee for the Cape Parry rocket.
†D means despun orbit; S means spinning orbit.

optical [OI] 6300 Å and ionosonde signatures and showed little temporal variation during the time of the flight. The 6300 Å ground-based scanning photometer showed the presence of a broad 6300 Å arc of about 1 kR north of the launch site.

The electron energy distribution between 0.03 and 18 keV was measured by an electron spectrometer mounted perpendicular to the spin axis. The orientation of the rocket during the flight made it possible to measure the electron flux at pitch angles between 70 and 110°. The particle data have been described in detail by McEwen (1977) and will only be briefly summarized here.

The latitudinal region crossed by the rocket may be described by three characteristic types of electron precipitation. The rocket first encountered a region of keV electrons with energy fluxes of a few erg cm^{-2}/s, then a zone of soft precipitation with highly variable flux identified as the polar cusp, and finally a region of very low energy flux corresponding to the polar cap. The directional energy flux measured along the trajectory is shown in Fig. 3. If isotropy over the downward hemisphere is assumed, these values should be multiplied by π to obtain the total energy flux. A limited region of strong precipitation was encountered near 77.2° invariant latitude where the flux reached a value of 8 erg cm^{-2}/s ster^{-1}. The characteristic

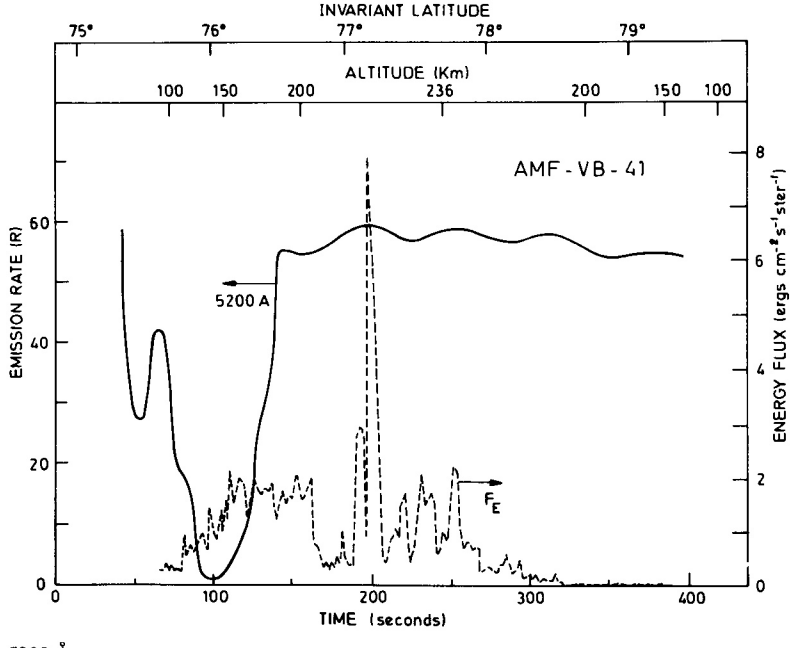

FIG. 3. NI 5200 Å EMISSION RATE AND TOTAL DIRECTIONAL ENERGY FLUX MEASURED ALONG THE ROCKET TRAJECTORY.

energy of the soft electrons in the cusp region is about 150 eV and hardens to about 650 eV inside the zone of increased precipitation.

The morphology of the 5200 Å measurements, shown in Fig. 3, is characterized by a sharp increase of the emission rate between $T + 100$ s and $T + 140$ s approximately, followed by an almost constant intensity of nearly 55 R. Superimposed on this slowly decreasing emission is a modulation with a period of about 63 s corresponding to the precession period of the rocket. The signal has been corrected for spikes and galactic background which was estimated to be 15 R in the 5200 Å channel. The absolute emission rates are deduced from the preflight laboratory calibration as well as in-flight calibration. The calibration procedure was described by Marette and Gérard (1976).

The enhanced 5200 Å emission plume suggests downwind transport of $N(^2D)$ by neutral winds or, as suggested by Shepherd *et al.* (1976), emission caused by antisunward convection of ions. The $N(^2D)$ has a radiative lifetime of 26 h. We examine the effect of winds on the $N(^2D)$ distribution in an attempt to account for the observed 5200 Å emission plume.

Model calculations

Measurements of the neutral wind were not made during the rocket flight. To obtain some indication of the neutral wind velocity and direction during the rocket flight we use the predictions by the NCAR thermospheric general circulation model. The model equations, parameterizations and results describing the solar driven circulation and temperature structure during equinox and solstice have been described by Dickinson *et al.* (1981). Roble *et al.* (1981) examined the effect of magnetospheric convection in altering the global circulation and temperature for equinox. The calculated temperature structure and circulation over the Northern Hemisphere polar cap for December solstice conditions at OOUT for geomagnetic quiet conditions is shown in Fig. 4. The contours give the perturbation temperature structure from a global mean value of 1100 K and the arrows give the circulation along the model $Z = +1$ surface of constant pressure at approximately 300 km. The rocket direction is shown by the solid line. The model calculations indicate that at this time there is a general flow along the rocket path with a maximum wind velocity of about 200 ms^{-1}. We thus parameterize the wind velocity in the two-dimensional numerical model by using the expression given by equation (1).

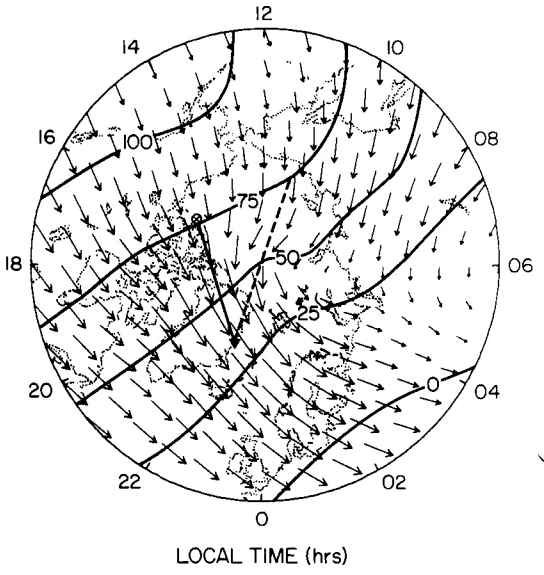

FIG. 4. CONTOURS OF PERTURBATION TEMPERATURE FROM A GLOBAL MEAN VALUE OF 1100 K AND HORIZONTAL WIND DISTRIBUTION ALONG A CONSTANT PRESSURE SURFACE NEAR 300 km CALCULATED FOR WINTER SOLSTICE AND QUIET, MAGNETIC ACTIVITY CONDITIONS (ROBLE *et al.*, 1982). THE MAXIMUM WIND VECTOR IS 205 ms^{-1}. The tracks of the rocket and AE-D trajectories are shown by the long solid line and short dashed line, respectively.

The electron particle flux spectra used in the model auroral calculation is given by equation (3). The values of α and F used to specify the particle flux along the rocket trajectory are shown in Fig. 5. The curves represent smooth profiles of the actual data that are used for modeling the event. In the early part of the rocket flight a hard energy flux was detected with an α of about 4. It decreased with distance along the rocket trajectory. The peak flux values were detected about 250 km from the launch site. Also shown in the figure is a plot of the total energy input by the particles. The calculated electron density using the distribution of α and F along the flight path is shown in Fig. 6. At low latitudes the particle distribution is hard and there is considerable enhancement of the electron density at low altitudes. At higher latitudes the particle spectrum softens considerably but the flux intensifies and a peak electron density of 5.4×10^6 cm^{-3} near 250 km is calculated. Near 78° latitude the particle flux decreases abruptly and the electron densities decrease to their background values in the region of the polar cap.

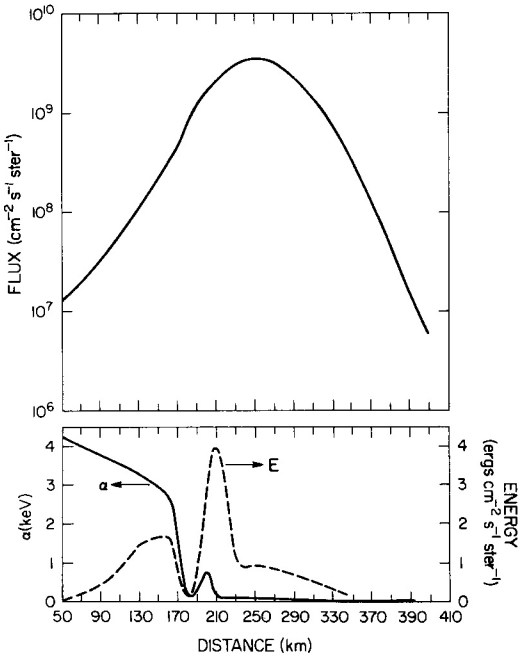

FIG. 5. ALPHA AND F PARAMETERS IN EQUATIONS (3) AND (4) USED TO SIMULATE THE PRECIPITATION DISTRIBUTION ALONG THE ROCKET FLIGHT.
The total energy input by the particles is also shown.

Without winds, the calculated distributions of NO, N(⁴S) and N(²D) are enhanced in the region where the rocket measured the enhanced electron flux distribution. The N(²D) distribution, calculated without winds is similar to the electron density distribution shown in Fig. 7; however, the peak N(²D) density is about 50 km lower in altitude than the peak electron density. The N(⁴S) distribution is also similar to the electron density distribution, although the peak N(⁴S) density is about 25 km lower than the N(²D) density. The NO density peaks in the lower thermosphere near 120 km.

We present two calculations to illustrate the effect of winds on the distribution of the minor neutral constituents for the rocket case. The first uses an exospheric wind speed, v_∞ in equation 1, of 100 ms^{-1} and the second uses 300 ms^{-1}. The results for the first case are shown in Figs. 7a, 7b and 7c and for the second in Figs. 7d, 7e and 7f. The winds transport the minor neutral constituents produced by the aurora downwind in both cases. The plume extends farther downstream for the case with the higher wind speed after 3 h of model integration time. The higher wind speed transports constituents much farther horizontally and as a result the number density near the vicinity of the aurora is smaller than in the low wind speed case. The vertical constituent profiles at high latitudes will depend not only on auroral production but also on the wind speed and direction.

The calculated total 5200 Å emission rate integrated upward from the height of the rocket trajectory is shown in Fig. 8 for four different wind speed cases along with the rocket measurements. The calculated emission rates agree reasonably well with the rocket measurements if a 150–200 ms^{-1} wind is assumed to be blowing through the cusp region and transporting N(²D) downstream. This wind speed is consistent with predictions from the NCAR thermospheric general circulation model shown in Fig. 4.

A perfect match between the observed and calculated 5200 Å distributions cannot be expected because of the following limitations:

1. The electron energy spectrum is measured from the rocket, thus, within the atmosphere. Any very soft component below the atmospheric energy cutoff would not be measured by the electron detectors and consequently would not be included in the model calculation.

2. The composition of the neutral atmosphere was not measured during the flight, and values from the MSIS model were adopted. There are indications in the literature that the high latitude thermosphere may be richer in O_2 and poorer in 0 than some current model atmospheres (Deans and Shepherd, 1978; Sharp *et al.*, 1979; Gérard and Rusch, 1979; Rusch and Gérard, 1980; Sharp, 1980). If this was the case during the rocket flight, high altitude quenching by atomic oxygen (reaction 6) would be reduced and the chemical lifetime

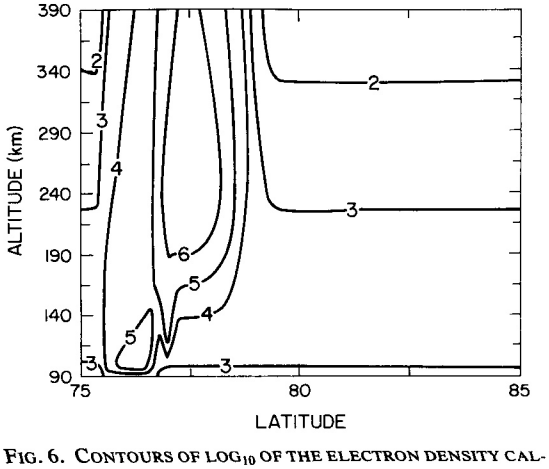

FIG. 6. CONTOURS OF LOG_{10} OF THE ELECTRON DENSITY CALCULATED IN THE MODEL OF THE ROCKET OBSERVATIONS.

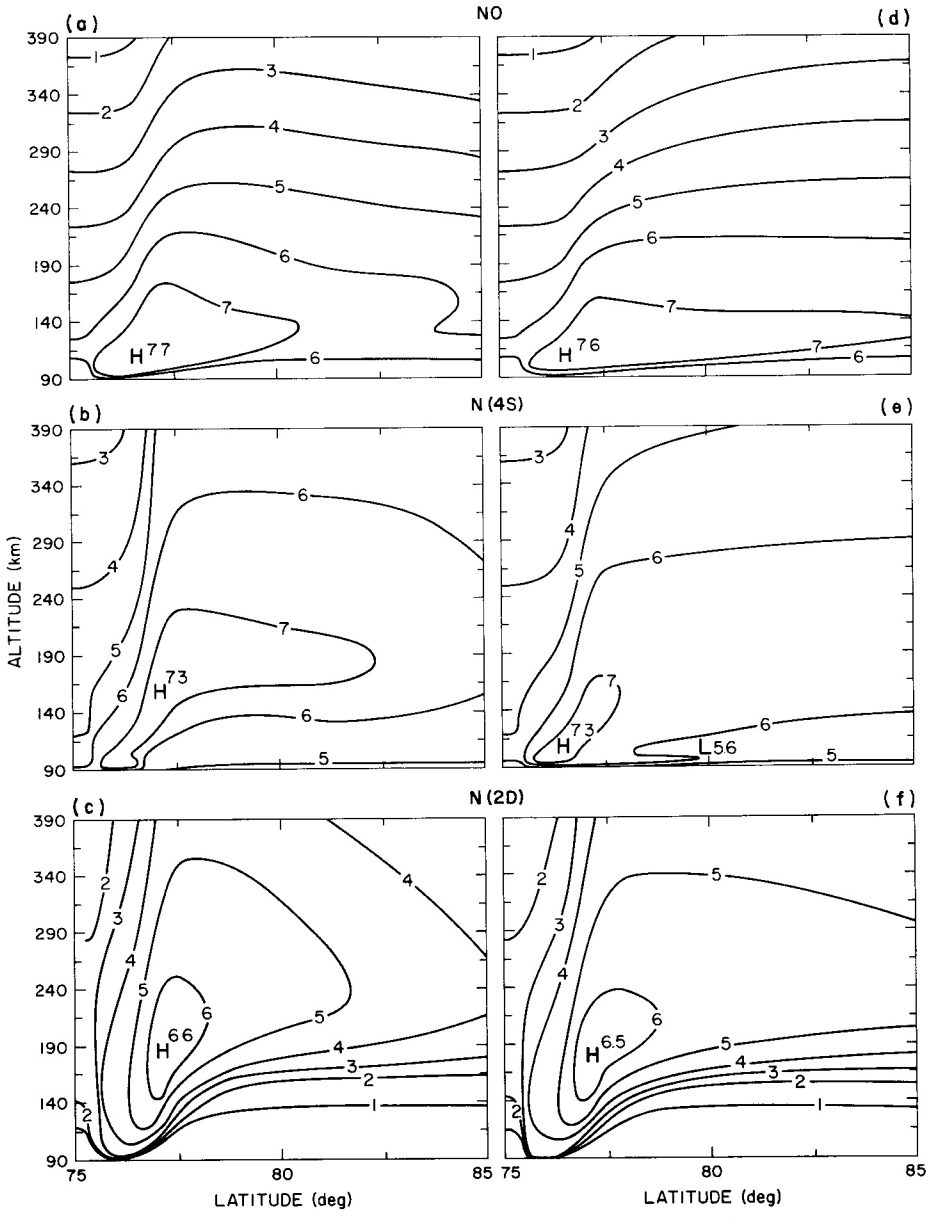

FIG. 7. CONTOURS OF CALCULATED LOG_{10} OF ODD NITROGEN DENSITIES AFTER 3 h OF AURORAL PRECIPITATION FOR THE ROCKET CASE: (a), (b) AND (c) WITH ASYMPTOTIC WIND VELOCITY OF 100 ms^{-1}; (d), (e) AND (f) WITH ASYMPTOTIC WIND VELOCITY OF 300 ms^{-1}.

of $N(^2D)$ would be larger than the value calculated in the model, allowing horizontal transport to be more effective.

3. Other mechanisms may be present to transport $N(^2D)$ or its precursors away from the precipitation region.

The fair agreement with the observations for reasonable values of the wind velocity indicates that transport by wind is probably taking place. If the chemical lifetime of $N(^2D)$ was considerably shorter than considered in the model the downwind plume would not develop as extensively. This would be the case, for example, if deactivation by atomic oxygen occurred with much higher efficiency as implied by the results of Davenport *et al.* (1976). However, the observations

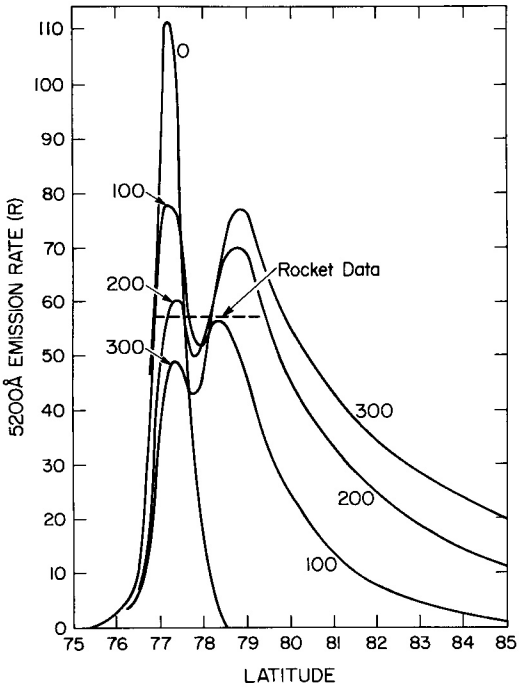

FIG. 8. COLUMN EMISSION RATE OF NI 5200 Å ABOVE THE ROCKET ALTITUDE CALCULATED WITH DIFFERENT WIND VELOCITIES (ms^{-1}).
The measured distribution is given by the dashed line.

would require an unreasonably high wind velocity if their quenching rate was adopted.

5. SATELLITE OBSERVATIONS OF N(²D) HORIZONTAL TRANSPORT

We examined the data base of the Visible Airglow Experiment (VAE) on board the Atmosphere Explorer satellites for evidence of horizontal transport of N(²D) from the 5200 Å high latitude emission. A general description of the VAE experiment was given by Hays *et al.* (1973a). The orbit of the AE-D satellite was polar at nearly constant local time. The VAE observations could be accurately corrected for galactic background during the high altitude portions of the orbits when the spacecraft was above the terrestrial airglow sources as described by Torr *et al.* (1977). However, the number of suitable orbits for this study was limited by the following constraints: (1) the observation mode had to be such that the 5200 Å filter was used with the wide-angle (6°) channel to obtain a sufficient signal to noise ratio (S/N), (2) perigee had to be located in the dark polar regions, and (3) the AE-D mission was fairly short-lived, due to technical problems in the spacecraft. Nevertheless, we were able to select three orbits and obtain supporting data from other instruments. These cases provide evidence for N(²D) emission out of the region of particle bombardment. Some characteristics of the three orbits are listed in Table 2.

Orbit AE-D 419

A portion of the upleg of orbit 419 is shown in Fig. 9. The observations were made in the despun mode in the night-side auroral zone of the Northern (winter) Hemisphere. The 5200 Å overhead vertical emission rate is plotted every 5.7 s. The sensitivity is 8.5 counts $Rayleigh^{-1}$ for the wide-angle channel used for these measurements. The error bars indicate the 1σ standard deviation. The directional energy flux F_E averaged over 15 s is also plotted for comparison. It was measured by a set of detectors, as a part of the low energy electron spectrometer (LEE), between 0.2 and 25 keV (Hoffman *et al.*, 1973a).

The precipitation region extends from $T =$ 67, 250–67,450 s approximately and consists of a strong but fairly narrow zone located at $\Lambda = 73°$ reaching 2.7 erg cm^{-2}/s $ster^{-1}$, followed by a wider and weaker maximum of about 1 erg cm^{-2}/s $ster^{-1}$ near $\Lambda = 65°$. The energy flux drops to very low values after 67,450 s. The 5200 Å column intensity follows the main features of the precipitation pattern. However, the spatial resolution of the VAE data used for this plot is about four times lower than the particle data. Consequently, some of the 5200 Å morphological features are smoothed in the other measurements. The 5200 Å emission shows an equatorward tail of a few Rayleighs extending far south of the southern boundary of the particle precipitation. The rapid increase of the spacecraft altitude after 67,520 s may partly obscure the effect of equatorward transport of N(²D) by neutral winds. In order to discriminate between the effects of neutral wind and ion drift, we have also plotted the $[NO^+]$ [e] product measured locally by the magnetic ion mass spectrometer (MIMS) (Hoffman *et al.*, 1973b). Again the measurements are averaged over a period of 15 s. If the 5200 Å emission measured away from the source region was produced by the dissociative recombination (reaction 11 of Table 1) of NO^+ ions formed by charge exchange of O^+ with N_2 (reaction 10), the 5200 Å volume emission rate would be proportional to this product. It is not possible to rule out the possibility of O^+ convection by the electric field at higher altitudes,

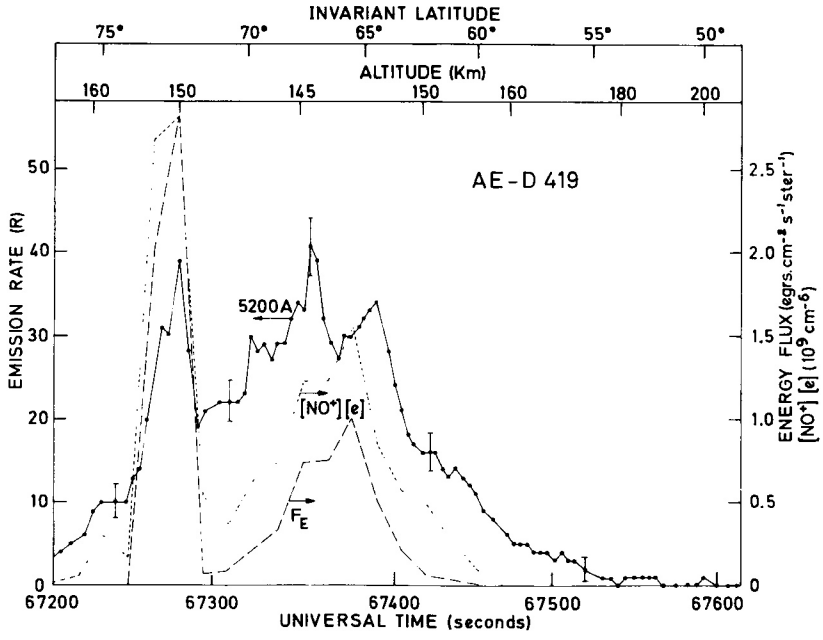

FIG. 9. MEASUREMENTS OF 5200 Å EMISSION RATE, TOTAL ELECTRON ENERGY FLUX, AND $[NO^+][e]$ PRODUCT MADE ON ORBIT AE-D 419.

which would not be measured locally by the ion mass spectrometer but which would affect the $N(^2D)$ slant intensity. However, another case at higher altitudes presented below does not show any convection effect either.

Orbit AE-D 491

Figure 10 shows similar observations made at higher altitudes in and south of the night-side auroral precipitation region. Between $T = 80{,}470$ and 80,600 s, the spacecraft crossed the night-side

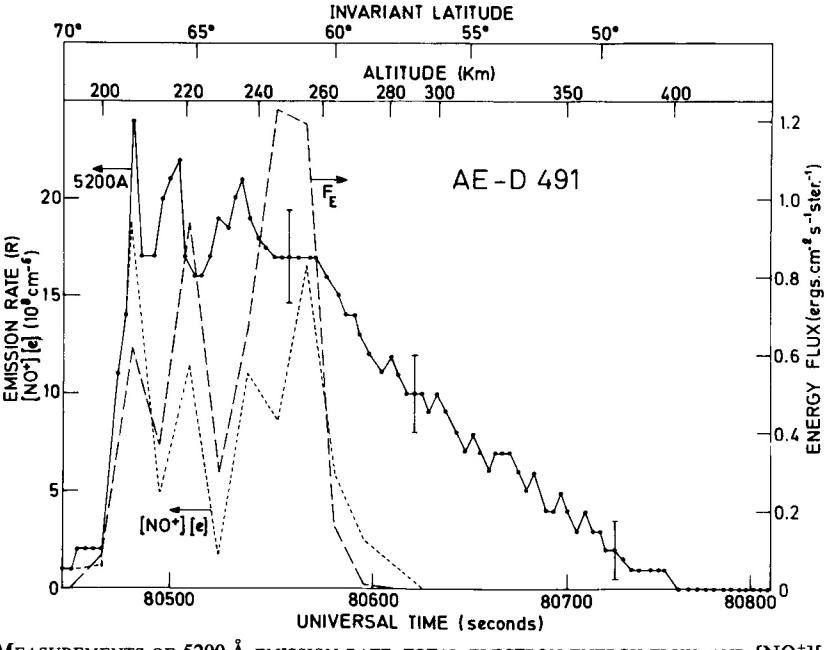

FIG. 10. MEASUREMENTS OF 5200 Å EMISSION RATE, TOTAL ELECTRON ENERGY FLUX, AND $[NO^+][e]$ PRODUCT MADE ON ORBIT AE-D 491.

auroral oval, as indicated by the fairly large energy flux that varied between 0.1 and 1.2 erg cm^{-2}/s ster^{-1} measured during the LEE experiment. The invariant latitude of the auroral precipitation ranged from 58 to 68°N. At lower latitudes the flux dropped rapidly below 0.01 erg cm^{-2}/s ster^{-1} as the spacecraft moved away from the auroral oval. However, a significant amount of 5200 Å emission was observed until $T = 80{,}760$ s. Farther south, the 5200 Å emission dropped to zero. The rapid cutoff of the particle precipitation at the equatorward boundary of the auroral zone makes it possible to determine the characteristic distance of the 5200 Å emission. The observed emission rate gradient is about 1.2 R degree^{-1} or 0.1 R km^{-1}. This gradient corresponds to a decrease in intensity by a factor of two over a horizontal distance of about 500 km, presumably under the effect of an equatorward neutral wind. The [NO$^+$][e] product is also plotted every 15 s. It follows fairly closely the energy flux variations but does not exhibit any long midlatitude tail as does the 5200 Å emission. This orbit represents the most dramatic evidence for horizontal transport of N(²D) in the night-side high latitude regions.

Orbit AE-D 494

Observations were made in the spinning mode on orbit 494. The spacecraft reached perigee only a short time after flying over the geographic North Pole ($T = 80{,}880$ s). The local solar time of the orbit is 10.6 h before and 22.6 h after passing over the geographic pole. The particle data shown in Fig. 11 indicate that most of the region near perigee was fairly free of energetic particles with the exception of a narrow zone of intense energy precipitation reaching 0.14 erg cm^{-2}/s ster^{-1} at $\Lambda = 78$°N. The actual width of this strong particle precipitation is less than the 15 s resolution used to plot the LEE data. The mean energy of the electrons measured in this zone is 1.2 keV. Consequently, the magnetic location and the characteristic energy of the precipitated electrons are such that we identify this narrow region as the day-side polar cusp.

The 5200 Å overhead brightness is measured once per rotation, i.e., every 15 s. The emission rate of the (0, 1) band of the N_2^+ first negative system is measured on the narrow-angle channel (1.5°) at the same rate with a sensitivity of 0.04 count Rayleigh.$^{-1}$ The intensity of this emission is proportional to the integrated N_2 dissociation and ionization rates above the satellite. Comparison of the three quantities shows that both optical emissions peak in the cusp precipitation region at 55 R for 5200 Å and 770 R for 4278 Å. The 4278 Å intensity drops to less than 10 R at 15,915 s and to 0 at 15,990 s. The energy flux measured in this orbit is plotted on a different scale than Figs. 9 and 10 since it is much smaller than that measured in the

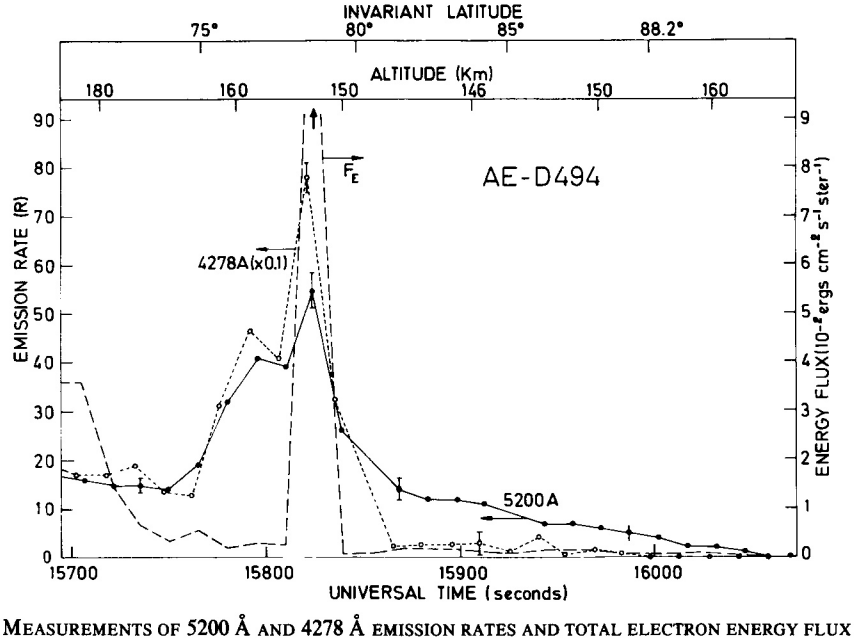

FIG. 11. MEASUREMENTS OF 5200 Å AND 4278 Å EMISSION RATES AND TOTAL ELECTRON ENERGY FLUX MADE ON ORBIT AE-D 494.

Hays, P. B., Carignan, G., Kennedy, B. C., Shepherd, G. G. and Walker, J. C. G. (1973a) The visible airglow experiment on Atmosphere Explorer. *Radio Sci.* **8**, 369.

Hays, P. B., Jones, R. A. and Rees, M. H. (1973b) Auroral heating and the composition of the neutral atmosphere. *Planet. Space Sci.* **21**, 559.

Hedin, A. E., Salah, J. E., Evans, J. V., Reber, C. A., Newton, G. P., Spencer, N. W., Kayser, D. C., Alcaydé, D., Bauer, P., Cogger, L. and McClure, J. P. (1977a) A global thermospheric model based on mass spectrometer and incoherent scatter data, MSIS 1, N_2 density and temperature. *J. geophys. Res.* **82**, 2139.

Hedin, A. E., Reber, C. A., Newton, G. P., Spencer, N. W., Brinton, H. C., Mayr, H. G. and Potter, W. E. (1977b) A global thermospheric model based on mass spectrometer and incoherent scatter data, MSIS 2, Composition. *J. geophys. Res.* **82**, 2148.

Heelis, R. A., Hanson, W. B. and Burch, J. L. (1976) Ion convection velocity reversals in the dayside cleft. *J. geophys. Res.* **81**, 3803.

Hoffman, R. A., Burch, J. L., Janetzbe, R. W., McChesney, J. F., Way, S. H. and Evans, D. S. (1973a) Low-energy electron experiment for Atmosphere Explorer-C and D. *Radio Sci.* **8**, 393.

Hoffman, J. H., Hanson, W. B., Lippincott, C. R. and Ferguson, E. E. (1973b) The magnetic ion mass spectrometer on Atmosphere Explorer. *Radio Sci.* **8**, 315.

Lindinger, W., Albritton, D. L., Fehsenfeld, F. C. and Ferguson, E. E. (1975) Laboratory measurements of the ionospheric O_2^+ ($X^2\pi_g$) and $O_2^+(a^4\pi_u)$ reactions with NO. *J. geophys. Res.* **80**, 3725.

Marette, G. and Gérard, J. C. (1976) Rocket borne baffled photometer: design and calibration. *Appl. Optics* **15**, 437.

McEwen, D. J. (1977) Electron precipitation observations from a rocket flight through the dayside auroral oval. *Planet. Space Sci.* **25**, 1161.

Mehr, F. J. and Biondi, M. A. (1969) Electron temperature dependence of recombination of O_2^+ and N_2^+ ions with electrons. *Phys. Rev.* **181**, 264.

Phillips, L. F. and Schiff, H. I. (1962) Mass spectrometer studies of atom reactions, 1. Reactions in the atomic notrogen–ozone system. *J. chem. Phys.* **36**, 1509.

Rees, M. H. (1969) Auroral electrons. *Space Sci. Rev.* **10**, 413.

Rees, M. H. and Roble, R. G. (1980) Effect of a horizontal wind on 1.27 μm auroral emission from $O_2(^1\Delta_g)$ molecules. *J. geophys. Res.* **85**, 4295.

Roble, R. G. and Rees, M. H. (1977) Time-dependent studies of the aurora: Effects of particle precipitation on the dynamic morphology of ionospheric and atmospheric properties. *Planet. Space Sci.* **25**, 991.

Roble, R. G. and Gary, J. M. (1979) The effect of horizontal transport on auroral NO densities. *Geophys. Res. Lett.* **6**, 703.

Roble, R. G., Dickinson, R. E. and Ridley, E. C. (1982) Global circulation and temperature structure of the thermosphere with high latitude plasma convection. *J. geophys. Res.* **87**, 1599.

Roble, R. G., Dickinson, R. E. and Ridley, E. C. (1982) The global circulation and temperature structure of the thermosphere for solstice conditions. *Planet. Space Sci.* (to be submitted).

Rusch, D. W., Stewart, A. I., Hays, P. B. and Hoffman, J. W. (1975) The NI (5200 Å) dayglow. *J. geophys. Res.* **80**, 2300.

Rusch, D. W. and Gérard, J. C. (1980) Satellite study of N(^{2}D) emission and ion chemistry in aurorae. *J. geophys. Res.* **85**, 1285.

Sharp, W. E., Rees, W. H. and Stewart, A. I. (1979) Coordinated rocket and satellite measurements of an auroral event, 2. The rocket observations and analysis. *J. geophys. Res.* **84**, 1977.

Sharp, W. E. (1980) Atomic oxygen in aurora. *EOS Trans. AGU* **61**, 1062.

Shepherd, G. G., Pieau, J. F., Creutzberg, F., McNamara, A. G., Gérard, J. C., McEwen, D. J., Delana, B. and Whitteker, J. H. (1976) Rocket and ground-based measurements of the dayside magnetospheric cleft from Cape Parry, N. W. T. *Geophys. Res. Lett.* **3**, 69.

Torr, M. R., Hays, P. B., Kennedy, B. C. and Walker, J. C. G. (1977) Inter-calibration of airglow observations with the Atmosphere Explorer satellite. *Planet. Space Sci.* **25**, 173.

Torr, D. G. and Torr, M. R. (1979) Chemistry of the thermosphere and ionosphere. *J. atmos. terr. Phys.* **41**, 797.

Torr, D. G., Torr, M. R., Brinton, H. C., Brace, L. H., Spencer, N. W., Hedin, A. E., Hanson, W. B., Hoffman, J. H., Nier, A. O., Walker, J. C. G. and Rusch, D. W. (1979) An experimental and theoretical study of the mean diurnal variation of O^+, NO^+, O_2^+ and N_2^+ ions in the mid-latitude F_1 layer of the ionosphere. *J. geophys. Res.* **84**, 3360.

Wilson, W. E. (1967) Rate constant for the reaction $N + O_2 \rightarrow NO + O$. *J. chem. Phys.* **46**, 2017.